Batteries & Supercaps

Research Article
doi.org/10.1002/batt.202500431

Chemistry Europe
European Chemical Societies Publishing

www.batteries-supercaps.org

From Neutral Zwitterion to Electroactive Disalt: Electrochemical Insights into Double Zwitterionic Viologens for Anion-Insertion Batteries

Alexia Rocheteau, Luisa Rzesny, Arvinder Singh, Thomas Devic, Mathias Hermann, Joël Gaubicher, Nicolas Dupré, Stéven Renault, Birgit Esser,* and Philippe Poizot*

In the quest for sustainable and metal-free energy storage systems, viologen-based materials offer exciting prospects as they are synthetically well accessible and show two reversible electrochemical processes with anion insertion. This study introduces and compares two π-extended viologen–carboxylate materials bearing double zwitterionic backbones as model compounds based on 1,1′-bis(4-carboxyphenyl)-4,4′-bipyridinium ([bcbp]): the neutral [bcbp] as a double zwitterionic molecule **(1)** and its corresponding $(Li)_2[bcbp](ClO_4)_2$ disalt **(2)**. The choice of these two materials for our electrochemical studies is motivated by the literature available on their synthesis routes and solid-state properties. Electrochemical tests in lithium half-cells revealed that compound **(1)** is initially inactive but gradually converts into the electroactive disalt **(2)** via spontaneous chemical insertion of $LiClO_4$ from the electrolyte. Compound **(2)** directly displays the expected reversible two-electron *p*-type mechanism involving perchlorate anion (de)insertion, while lithium ions act as spectator species. The system delivers stable cycling performance and high coulombic efficiency, supporting the interest of viologen-based zwitterionic salts as host material for negative electrode application in anionic rocking-chair organic batteries. The bipyridinium-bis(carboxylate) radical ((Li)[bcbp]$^{\bullet}$ **(3)**) formed during our synthesis optimizations is likewise electrochemically assessed. This fundamental work highlights the tunability of double zwitterionic viologens as molecular platforms to promote optimized *p*-type negative electrode materials.

1. Introduction

N,*N*′-Disubstituted-4,4′-bipyridinium salts, commonly known as viologens, a term introduced by Michaelis in 1932,[1] constitute a prominent class of functional compounds whose relevance extends well beyond their interest as synthons in cyclization reactions in organic chemistry.[2] Originally developed for antibacterial and herbicidal applications, viologens have since been repurposed as versatile molecular components in a wide range of advanced materials and devices. Belonging to the *p*-type redox-active systems (or "system B" according to Hünig's classification[3,4]), viologens typically exhibit a reversible, two-step redox process ($V^{2+} \rightleftarrows V^{+} \rightleftarrows V^{0}$),[5] which can be activated by electrical, chemical, or optical stimuli. The first one-electron reduction converts the pale yellow or off-white dication (V^{2+}) into a brightly colored radical cation (V^{+}), typically purple or green. A second reduction yields a colorless neutral species (V^{0}). This dynamic redox behavior forms the basis of their utility in electrochromic devices, enabling reversible visual switching, and supports their integration into memory elements, transistors, molecular machines, sensors, and so on.[6] Due to their intrinsically electron-deficient character, viologens readily engage in charge–transfer interactions with electron-rich counterparts. This property facilitates their incorporation into supramolecular architectures, including host–guest complexes and mechanically interlocked molecules.[7,8]

Among *p*-type redox systems, viologens work at relatively low potential, making them well suited for use as a negative electrode in electrochemical devices. Electrochromic devices represent the earliest application of viologens as negative electrode materials, a choice driven by the well-defined and distinguishable absorption spectra corresponding to their three redox states.[9] This optical responsiveness continues to be the subject of active research and technological development for flexible electrochromic devices.[10]

Beyond their well-established role in electrochromic systems, viologen derivatives have also emerged as promising candidates for electrochemical energy storage, particularly as negolytes in redox flow batteries, as highlighted in a recent review.[11] In contrast, their use as solid-state negative electrode materials remains largely unexplored, despite promising potential. However, if properly tailored for sufficient chemical stability in the solid state paired with low redox potential operation, viologen-based electrodes could open the door to the development of anionic

A. Rocheteau, A. Singh, T. Devic, J. Gaubicher, N. Dupré, S. Renault, P. Poizot
CNRS
Institut des Matériaux de Nantes Jean Rouxel
IMN
Nantes Université
F-44000 Nantes, France
E-mail: philippe.poizot@cnrs-imn.fr

L. Rzesny, M. Hermann, B. Esser
Institute of Organic Chemistry II and Advanced Materials
Ulm University
Albert-Einstein-Allee 11, 89081 Ulm, Germany
E-mail: birgit.esser@uni-ulm.de

Supporting information for this article is available on the WWW under https://doi.org/10.1002/batt.202500431

Research Article
doi.org/10.1002/batt.202500431
Chemistry Europe
European Chemical Societies Publishing

rocking-chair batteries,[4] a conceptual breakthrough toward fully metal-free, molecular battery technologies. In the limited number of studies addressing the development of all-organic anionic batteries,[12–15] we have made significant contributions to advancing this emerging field in recent years.[16–20]

Building on previous investigations reported in 2019,[16] this study aims to deepen the understanding of electrochemical storage mechanisms in viologen-dicarboxylate derivatives, explored as insertion-type materials with the objective in the near future of developing efficient negative *p*-type electrodes centered on the viologen redox unit. To this end, we selected a π-extended model system based on the redox-active molecule 1,1′-bis(4-carboxyphenyl)-4,4′-bipyridinium, chosen for the wealth of literature and well-characterized properties of related compounds.[21–25] In fact, these materials are particularly well documented due to their unique photochromic, piezochromic, and hydrochromic behaviors in the solid state, making them a rare and valuable example within the broader class of organic functional materials. In line with a previous study,[16] we chose to install phenyl rings between the bipyridinium core and the carboxylate groups to enhance the stability of the resulting species (**Scheme 1**). At the molecular level, this *N*-arylation prevents the known viologen degradation mechanism, which involves nucleophilic cleavage of the *N*-substituent.[26] Among the known frameworks based on 1,1′-bis(4-carboxyphenyl)-4,4′-bipyridinium, we selected and synthesized two representative compounds (Scheme 1): 1) the double zwitterionic lithium perchlorate disalt, $(Li)_2[bcbp](ClO_4)_2$, for which a reversible two-electron reaction with a concomitant ClO_4^- (de) insertion process was anticipated, and 2) the neutral double zwitterionic molecule [bcbp], for which no *p*-type electrochemical activity was expected, although a possible *n*-type response could not formerly be excluded by "self-doping" mechanism.[27] Both compounds were structurally characterized and electrochemically evaluated in lithium half-cells to assess their suitability for energy storage applications. Our compounds, which formally belong to the family of *N*-arylated viologens,[28] bear phenyl substituents with electron-withdrawing carboxylate groups in the *para*-position; this type of π-extension was therefore expected to affect the redox potential differently from the core-extended viologens reported by Kato et al.,[29] where the insertion of aromatic rings into the viologen backbone induces charge-separation effects.

2. Results and Discussion

To synthesize the two target compounds **(1)** and **(2)**, we designed a strategy guided by previously reported methodologies based on 1,1′-bis(4-carboxyphenyl)−4,4′-bipyridinium dichloride, hereafter referred to as $(H)_2[bcbp](Cl)_2$, as the fundamental building block (**Scheme 2**). $(H)_2[bcbp](Cl)_2$ is synthetically accessible through the Zincke reaction based on *N*,*N*′-quaternization of 4,4′-bipyridine, as commonly described in the literature.[21–25] Experimental details and analytical data are provided in Figure S1–S7 and Table S1, Supporting Information.

2.1. Synthesis, Characterization, and Electrochemical Behavior in Li Half-Cells of the Viologen–Carboxylate Double Zwitterionic Molecule (1)

While single crystals of zwitterionic [bcbp] × $6H_2O$ have been reported,[21,30,31] no procedure for obtaining this phase as a powder has been clearly described. We therefore adapted the method of Sui et al.[31] based on slow cooling of a NaOH-neutralized aqueous solution of $(H)_2[bcbp](Cl)_2$ (Scheme 2; see Experimental Section). The purity of the obtained compound was confirmed using Fourier transform infrared (FTIR) spectroscopy (**Figure 1**a, black) and powder X-ray diffraction (PXRD; Figure 1c, black and Figure S8, Supporting Information), and the hydration level was verified by thermogravimetric analysis (TGA) and differential scanning calorimetry (DSC) (Figure 1b, black). As expected, the TGA curve exhibits two successive and asymmetric weight losses occurring between 25 and ≈190 °C, which are associated with two endothermic phenomena on the DSC trace. The total weight loss of ≈21.3% is in excellent agreement with the theoretical value expected for the loss of six water molecules ($\Delta m_{theo.}$ = 21.4%).

The corresponding anhydrous phase [bcbp], referred to as **(1)**, was subsequently obtained through a gentle and controlled

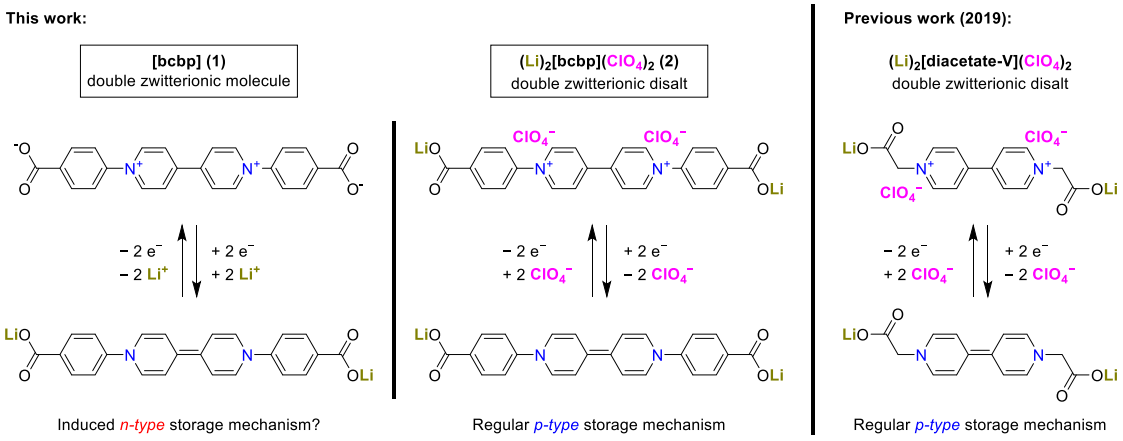

Scheme 1. Envisioned electrochemical reactivity of the two target compounds and previously studied viologen–carboxylate material.[16]

Research Article
doi.org/10.1002/batt.202500431
Chemistry Europe
European Chemical Societies Publishing

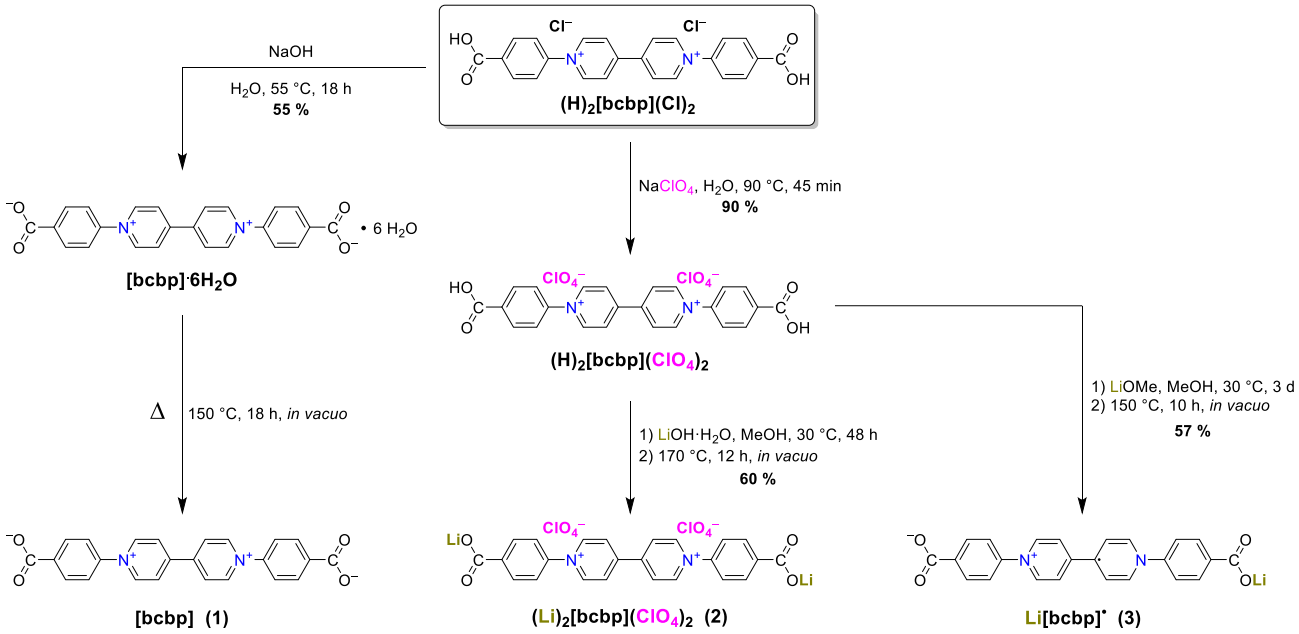

Scheme 2. Synthesis routes used to prepare the target compounds **(1)** and **(2)** with the radical **(3)** isolated during the experimental study.

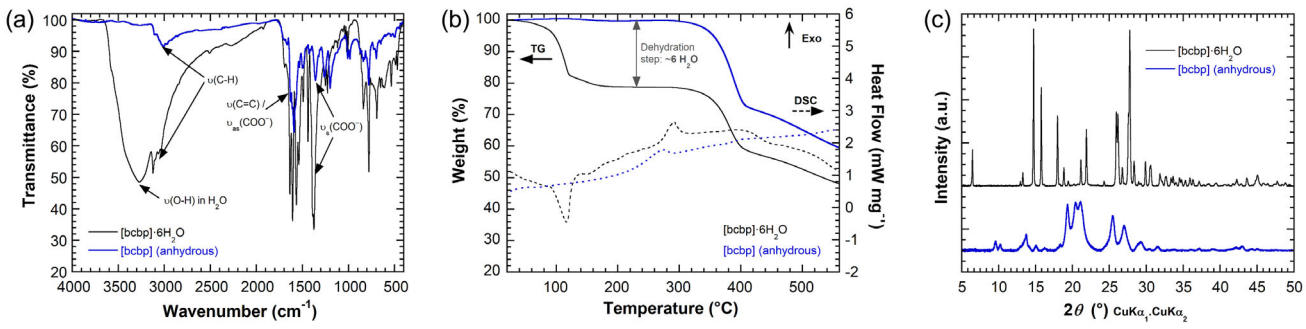

Figure 1. Comparative characterization by a) FTIR spectroscopy, b) TGA (solid lines)/DSC (dashed lines), and c) PXRD, confirming the formation of pure anhydrous [bcbp] **(1)** (blue) after controlled dehydration of the pristine [bcbp] × $6H_2O$ phase (black) at 150 °C.

dehydration process at 150 °C under vacuum since an exothermic phenomenon beyond 250 °C was observed on the DSC trace, presumably associated with the onset of the zwitterion decomposition (Figure 1b). Note that obtaining the anhydrous phase is particularly important for battery applications, as residual water can interfere with electrode stability, electrolyte compatibility, and the reproducibility of electrochemical performance. The completeness of the dehydration step was again confirmed by FTIR spectroscopy, PXRD, and TGA-DSC analyses (Figure 1, blue lines), which were in line with the literature data.[31] PXRD data revealed the expected phase transformation upon heating to 150 °C, marked by the appearance of new but broader and less intense diffraction peaks indicating a substantial loss of crystallinity after dehydration (Figure 1c). However, the persistence of distinct diffraction lines suggests that long-range structural coherence is retained. The observed decrease in crystallinity is likely due to the breakdown of the hydrogen-bonding network, which is essential for maintaining the structural integrity of the hexahydrated phase. scanning electron microscopy (SEM) images reveal that the [bcbp] × $6H_2O$ zwitterion powder is composed of micron-sized platelet agglomerates, which appear unchanged after dehydration (Figure S9, Supporting Information).

The electrochemical behavior of [bcbp] was evaluated in lithium half-cells using 1 M $LiClO_4$ in propylene carbonate (PC) as the electrolyte under galvanostatic cycling, in line with our previous investigations on bipyridinium dicarboxylate salts as organic electrode-active materials.[16] Composite electrodes were prepared without binder by mixing 67 wt% of the active material **(1)** with 33 wt% of conductive carbon (KB600). **Figure 2**a shows the corresponding galvanostatic cycling curves with an overlay of the first 50 cycles. Initially, the reduction of the double zwitterionic molecule **(1)** leads to a nearly negligible capacity. However, upon continued cycling, a progressive increase in capacity is observed, accompanied by the gradual emergence of the characteristic two-step reversible steps typical of viologen-based systems, centered at ≈2.8 and ≈2.4 V vs. Li^+/Li in the present case, respectively.

Research Article
doi.org/10.1002/batt.202500431
Chemistry Europe
European Chemical Societies Publishing

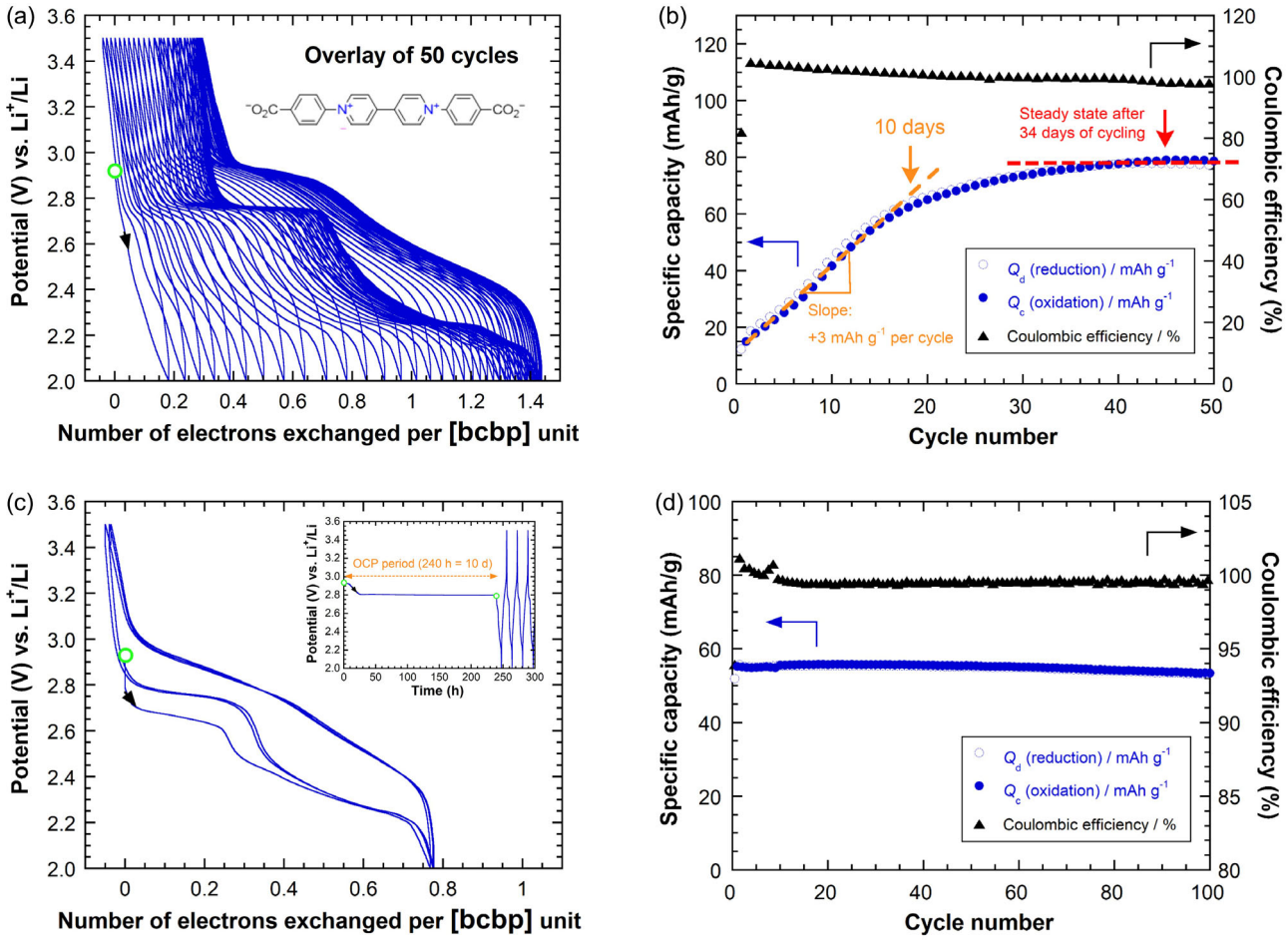

Figure 2. a) Typical potential-composition cycling curves of a Li half-cell using anhydrous [bcbp] double zwitterion **(1)** as the active material in 67 wt% mixed with 33 wt% KB600, showing a continuous activation of the cell capacity (cycling rate: C/20, 1 e^- exchanged per [bcbp] in 10 h, 6.8 mA g^{-1}; electrolyte: 1 M $LiClO_4$ in PC; M = 396.40 g mol^{-1}). b) Corresponding specific capacity retention curves together with the coulombic efficiency. c) Identical galvanostatic cycling protocol to (a), except for the application of a prolonged OCP period of 240 h (10 days) before initiating the first discharge (reduction) step. The green circles indicate the starting OCP value. d) Corresponding specific capacity retention curves together with the coulombic efficiency.

This peculiar electrochemical behavior suggests an activation process in which the material probably undergoes structural or electrochemical modifications over time. The corresponding capacity retention curve highlights the activation behavior of the electrode by exhibiting a two-stage evolution (Figure 2b): an initial activation phase over the first 20 cycles (≈10 days, highlighted in orange), during which the specific capacity increases almost linearly at an average rate of ≈3 mAh g^{-1} per cycle, followed by a stabilization phase. The steady-state capacity is reached after ≈34 days (≈45 cycles, highlighted in red) of cycling with very good coulombic efficiency, indicating highly reversible electrochemical processes with minimal parasitic reactions or capacity fading. To investigate the nature of this activation observed during initial cycles, a second experiment was performed in which the first reduction step was intentionally delayed by maintaining the cell under open-circuit potential (OCP) for 10 days prior to cycling. Under these conditions, the expected electrochemical characteristic features of viologen-based redox systems emerged immediately, with no apparent activation period (Figure 2c). This result confirms that the previously observed activation process is time-dependent and purely chemical in nature, presumably associated with the spontaneous chemical insertion of $LiClO_4$ into compound the [bcbp] framework, leading to the *in situ* formation of the double zwitterionic disalt **(2)**. Note that the number of electrons exchanged per [bcbp] unit is lower than expected (0.8 instead of 2 in Figure 2c), likely due to partial solubilization of [bcbp] in the liquid electrolyte or incomplete conversion of compound **(1)** into **(2)**. As a result, only ≈55 mAh g^{-1} is delivered, compared to the theoretical capacity of 135.6 mAh g^{-1}; nevertheless, the system exhibits excellent cycling stability over 100 cycles (Figure 2d).

In summary, the series of electrochemical cycling tests indicates that the double zwitterionic molecule **(1)** is electrochemically inactive and must be converted into the double zwitterionic disalt **(2)** to enable the normal operation of a *p*-type electrochemical system,[4] in which reduction leads to the electrochemical extraction of anions ([bcbp] does not contain any anionic species in its structure). In other words, no *n*-type electrochemical pathway occurs (Scheme 1). This observation was further supported by a supplementary electrochemical cycling test using lithium

poly(4-styrenesulfonyl(trifluoromethylsulfonyl)imide) as the electrolyte, a single-ion conducting electrolyte (SICE) dissolved in PC.[32] Basically, SICEs are designed to selectively transport lithium ions (Li^+), while the anionic species remain covalently bound to the polymer backbone.[33,34] Due to their bulky polymeric polyanion structure, no chemical insertion into the [bcbp] structure is possible, thereby suppressing possible *p*-type electrochemical reactivity, while still allowing in principle the *n*-type electrochemical mechanism. However, only residual reversible capacity was observed after several cycles. Altogether, these results led us to focus our attention on the double zwitterionic lithium perchlorate disalt, $(Li)_2[bcbp](ClO_4)_2$.

2.2. Synthesis, Characterization, and Electrochemical Behavior in Li Half-Cells of the Viologen–Carboxylate Double Zwitterionic Disalt (2)

For the synthesis of the viologen–carboxylate double zwitterionic disalt **(2)**, a literature known anion exchange from $(H)_2[bcbp](Cl)_2$ to $(H)_2[bcbp](ClO_4)_2$ was performed in a first step with 90% yield[35] (Scheme 2). Experimental and analytical details for $(H)_2[bcbp](ClO_4)_2$ are provided in Figure S10–S13, Supporting Information. We then searched for neutralization conditions that would provide us with the doubly lithiated compound. Based on our experience,[36,37] neutralization with $LiOH{\cdot}H_2O$ in an alcoholic medium has proven to be an effective method for the preparation of various conjugated lithium carboxylates. Following a series of preliminary experiments, the $LiOH{\cdot}H_2O$/methanol system was selected, and the second target compound $(Li)_2[bcbp](ClO_4)_2$ **(2)** was obtained in good yield (see Experimental Section). Similar to compound **(1)**, the resulting yellow/brown solid after neutralization was obtained in a solvated form, as evidenced by FTIR spectroscopy (**Figure 3**a), which revealed a broad band at 3400 cm^{-1} attributed to O–H vibrations, and further confirmed by TGA/DSC measurements (Figure 3b). Indeed, the thermogravimetric curve shows a weight loss occurring between 25 and ≈160 °C, corresponding to an endothermic event observed on the DSC trace. After annealing at 170 °C under vacuum, both FTIR measurement and TGA confirmed that the desolvated form of **(2)** was successfully obtained, while liquid ^1H and ^{13}C NMR confirmed the preservation of the molecular backbone (Figure S14–S15, Supporting Information). Direct comparison of the two IR spectra first reveals the presence of perchlorate ion vibration band ($\nu(ClO_4^-)$) around 1100 and 620 cm^{-1} in both the solvated and desolvated forms, confirming the formation of the expected salt. Moreover, the minimal spectral changes upon drying suggest that the structural framework remains unchanged during desolvation, consistent with observations in our previous work.[16] However, PXRD analysis revealed that the pristine disalt exhibited significantly lower crystallinity compared to the zwitterionic [bcbp] × $6H_2O$ on the one hand but also when compared to its "aliphatic" counterpart $(Li)_2$[diacetate-V]$(ClO_4)_2$. Upon thermal treatment, the diffraction pattern indicated that the material becomes highly disordered, approaching an amorphous state (Figure 3c). SEM images show that the as-prepared zwitterionic disalt **(2)** has a platelet-like, lamellar morphology with numerous agglomerates. After desolvation, a reduction in particle size is mainly observed (yielding micron-sized particles), arising from the breaking of agglomerates (Figure S16, Supporting Information).

The electrochemical behavior of the viologen–carboxylate double zwitterionic disalt **(2)** was also evaluated by galvanostatic cycling versus lithium in a half-cell configuration as described for **(1)**. This time, without any delay, the recorded cycling curves (**Figures 4**a,b) clearly exhibited the typical two-step reversible cycling profile, as previously observed for compound **(1)**, centered at ≈2.8 and ≈2.4 V vs. Li^+/Li. These electrochemical events can be attributed to the successive formation of the radical cation and the fully reduced neutral species ($V^{2+} \rightleftarrows V^{+} \rightleftarrows V^0$), respectively. Coulometric measurements indicate an average of ≈1.9 electrons exchanged per [bcbp] unit during the first reduction process, followed by an increase to ≈2 electrons per unit in subsequent cycles (Figure 4a). This behavior suggests improved accessibility of redox-active sites and is consistent with the sustained capacity retention observed upon extended cycling at C/20. To better grasp the shared electrochemical features, Figure 4c shows the galvanostatic reduction/oxidation profiles of the two synthesized viologen-based compounds: [bcbp] **(1)** (blue curve, with cycle no. 50 chosen as representative of the steady state) and $(Li)_2[bcbp](ClO_4)_2$ **(2)** (green curve, cycle no. 5), plotted against normalized capacity (0–2 electrons per [bcbp] unit). The close resemblance of the profiles as well as the associated differential capacity plot (d*Q*/d*E*) confirms the presence of nearly identical electrochemical behavior,

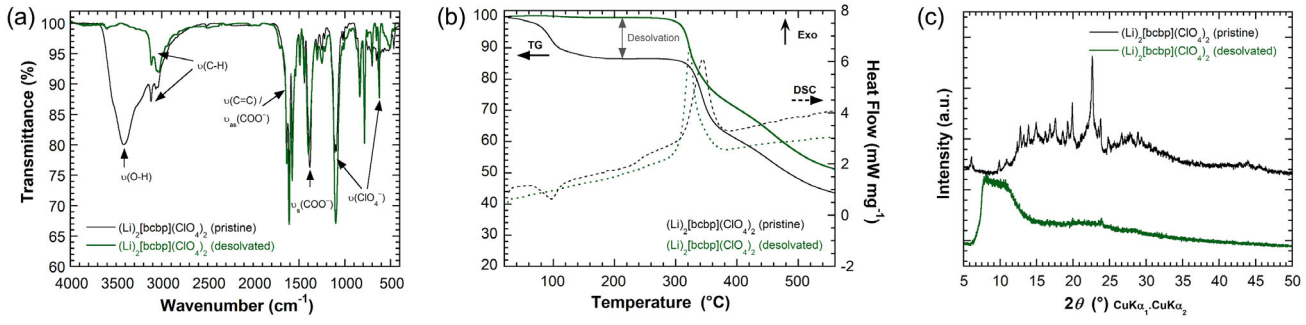

Figure 3. Comparative characterization of $(Li)_2[bcbp](ClO_4)_2$ after the neutralization step (pristine, black) and after annealing (desolvated, green) by a) FTIR spectroscopy, b) TGA (solid lines)/DSC (dashed lines), and c) PXRD of the double zwitterionic disalt powder $(Li)_2[bcbp](ClO_4)_2$ **(2)** obtained after acid–base neutralization (pristine, black) and after controlled dehydration at 170 °C (desolvated, green).

Research Article
doi.org/10.1002/batt.202500431
Chemistry Europe
European Chemical Societies Publishing

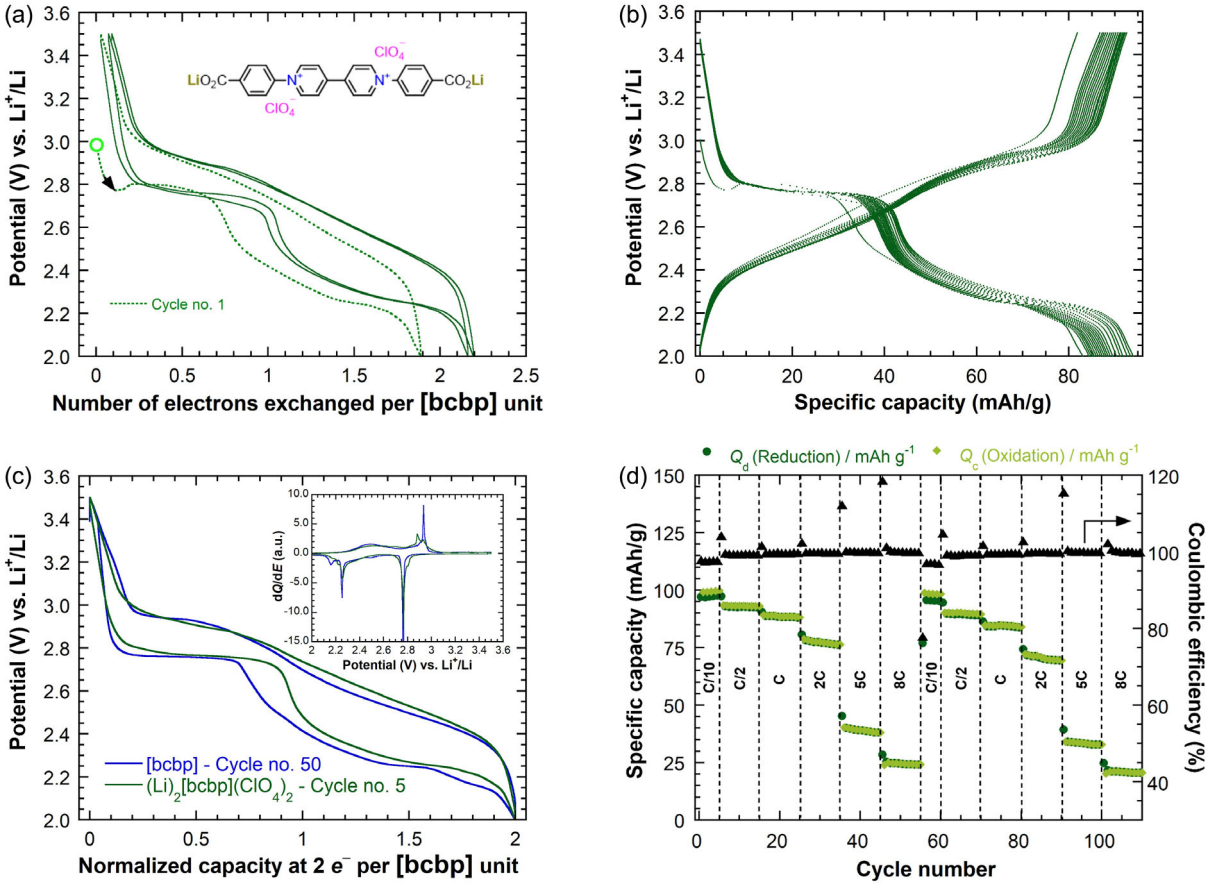

Figure 4. a) Typical potential-composition cycling curves recorded in a Li half-cell using the $(Li)_2[bcbp](ClO_4)_2$ disalt **(2)** as the active material in 67 wt% mixed with 33 wt% KB600 (cycling rate: C/20, 1 e^- exchanged per [bcbp] in 10 h, 4.4 mA g^{-1}; electrolyte: 1 M $LiClO_4$ in PC; M = 609.18 g mol^{-1}). The first cycle is shown as a dotted line, and the green circle marks the initial OCP. b) Corresponding potential–capacity curves over the first 25 cycles. c) Comparison after normalization at two electrons per [bcbp] unit of cycle 50 (blue) extracted from Figure 2a by using [bcbp] as the active material with cycle 5 (green) extracted from (b) by using $(Li)_2[bcbp](ClO_4)_2$ as the active material highlighting their remarkably similar electrochemical behavior. The inset displays the corresponding differential capacity plots (dQ/dE), further emphasizing the comparable electrochemical features. d) Specific capacity retention curves together with the coulombic efficiency obtained for different cycling rates ranging from C/10 to 8C for $(Li)_2[bcbp](ClO_4)_2$.

supporting the hypothesis reported above that the double zwitterionic molecule **(1)** gradually converts into the corresponding double zwitterionic disalt **(2)** upon contact with the electrolyte. When compared with the electrochemical features of $(Li)_2$[diacetate-V]$(ClO_4)_2$,[16] $(Li)_2[bcbp](ClO_4)_2$ exhibits a higher average operating potential, as highlighted in Figure S17, Supporting Information. This phenomenon can be attributed to the electron-withdrawing carboxylate groups, which are conjugated with the phenyl substituents in contrast to $(Li)_2$[diacetate-V]$(ClO_4)_2$ with methylene spacers, inhibiting π-conjugation. This shows that—as opposed to other instances of π-extension—in our case, the electron-withdrawing character of the carboxylate groups dominates.

Figure 4d shows the rate performance of compound **(2)** under galvanostatic cycling up to 8C: five initial cycles at C/10 followed by ten cycles each at C/2, C, 2C, 5C, and 8C, respectively, with the whole sequence repeated once. At the lowest current rate (C/10), the compound delivers an initial capacity close to or slightly above the theoretical value of 88 mAh g^{-1}, confirming efficient utilization of the redox-active centers. Upon increasing the rate, a progressive and reasonable decline in capacity is observed, dropping to ≈76 mAh g^{-1} at 2C rate while the coulombic efficiency remains remarkably stable and close to 100% throughout all cycles and current regimes, indicating highly reversible electrochemical processes and minimal parasitic reactions. With increasing rate up to 8C (0.7 A g^{-1}), the material still delivers a significant capacity (≈25 mAh g^{-1}) despite the very high current applied. When the rate is returned to C/10 after 55 cycles under such increasing cycling rates, the initial capacity is almost fully recovered. These results demonstrate not only stable cycling but also a remarkable ability of the material to sustain charge storage even under fast-rate conditions, an expected behavior for *p*-type electrode materials.

It is worth emphasizing that during our preliminary experiments aimed at identifying the optimal neutralization conditions for $(H)_2[bcbp](ClO_4)_2$ to produce the corresponding dilithium salt, we also explored the potential use of lithium methoxide (LiOMe) in methanol as a lithiated base building on the successful synthesis of several lithiated salts[38–40] in an argon-filled glovebox. However, with $(H)_2[bcbp](ClO_4)_2$, we observed the formation of a blue/violet solid, which is the characteristic color typically

Research Article
doi.org/10.1002/batt.202500431
Chemistry Europe
European Chemical Societies Publishing

associated with the radical form of viologens, suggesting the formation of the bipyridinium-bis(carboxylate) radical species ((Li)[bcbp]$^{\cdot}$) **(3)** (see Supporting Information). FTIR spectroscopy supported this hypothesis by showing that the characteristic perchlorate band at 1070 cm^{-1} was completely absent (Figure S18, Supporting Information), unlike in the spectrum of the $(H)_2$[bcbp]$(ClO_4)_2$ disalt. The spectrum also closely matched that of the [bcbp] zwitterion molecule, particularly with the two bands at ≈1260 and 1200 cm^{-1}, respectively, further supporting the proposed structure (Scheme 2). In addition, energy-dispersive X-ray spectroscopy (EDX) analysis confirmed the absence of chlorine in the sample. The explanation could be found in the ultrafast photoreduction of viologens in methanol reported by Kohler and co-workers.[41] Upon light exposure and under an inert atmosphere, the viologen dication (V^{2+}) is promoted to an excited state (V^{2+}*), which markedly increases the formal redox potential of the V^{2+}/V^{2+}* redox couple, rendering it more positive than that of the formaldehyde/methanol redox system. Consequently, the photoexcited dication undergoes spontaneous reduction by methanol to form the corresponding radical species (V^{+}). Another proof was given by the galvanostatic cycling assessment in a Li half-cell (Figure S19, Supporting Information). First, the measured OCP value (2.77 V vs. Li^+/Li) falls between the two redox steps observed during cycling of $(Li)_2$[bcbp]$(ClO_4)_2$ **(2)** (Figure 4b), consistent with an intermediate radical state. Second, independent cycling experiments starting with oxidation or with reduction yielded a reversible electrochemical response with approximately the one-electron theoretical capacity.

2.3. Probing the Electrochemical Reversibility of Perchlorate Extraction in (2) by Ex Situ FTIR and MAS-NMR

Based on our previous work on this topic,[16] the reversibility of the solid-state perchlorate ion extraction in the $(Li)_2$[bcbp]$(ClO_4)_2$ host material **(2)** was investigated by means of ex situ FTIR and MAS-NMR spectroscopies (**Figure 5**). When used in combination, these techniques are particularly well suited for probing this class of *p*-type active electrode materials. Three key points from the first electrochemical cycle were selected for the FTIR investigation (Figure 5a,b). The set of IR spectra provides clear evidence for a reversible anion insertion mechanism. The characteristic ClO_4^- vibrational band at 1070 cm^{-1} progressively diminishes during the discharge (reduction) step, indicating the extraction of perchlorate anions from the host material. Upon charging (oxidation), this band gradually reappears, confirming the reinsertion of the anions. It is worth noting that a residual intensity of the ClO_4^- band persists, consistent with the slightly lower capacity observed in the cell (1.85 equivalents extracted vs. the expected 2).

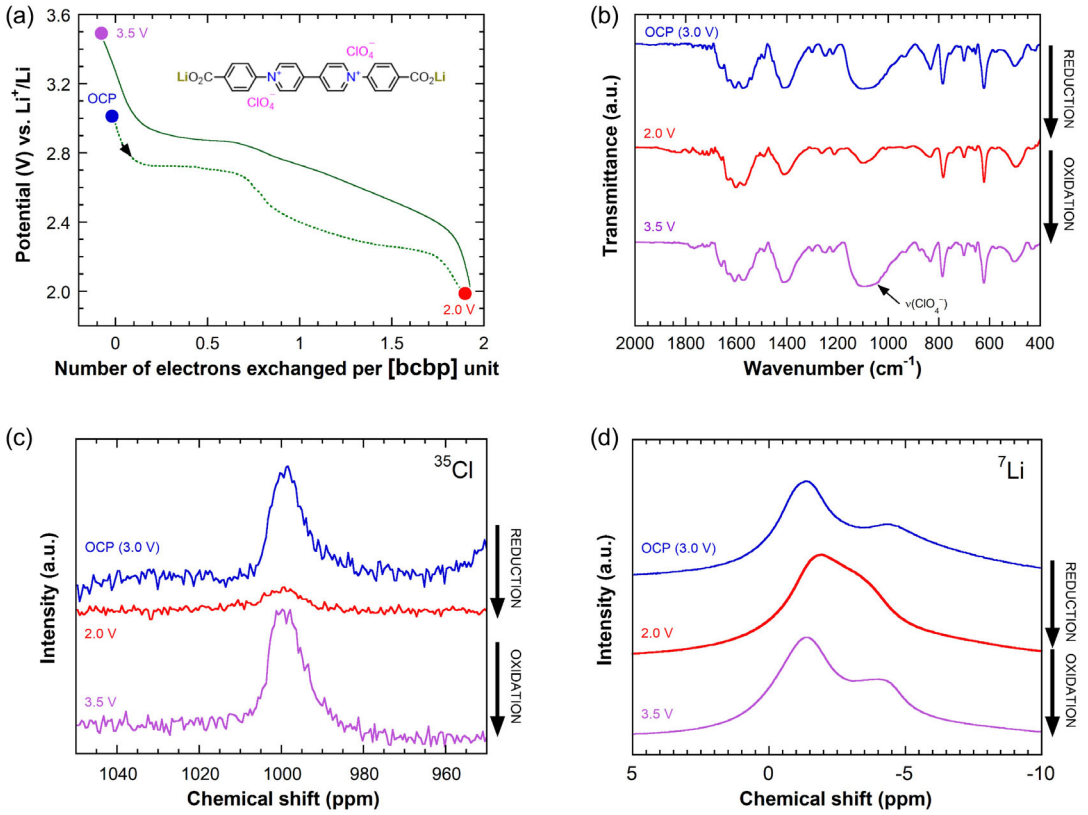

Figure 5. Ex situ FTIR and MAS-NMR studies of the solid-state perchlorate ion (de)insertion in the host material $(Li)_2$[bcbp]$(ClO_4)_2$ **(2)**. a) Typical first galvanostatic cycle profile of $(Li)_2$[bcbp]$(ClO_4)_2$ measured in a lithium half-cell using 33 wt% KB600 (cycling rate: C/20, 1 e^- exchanged per [bcbp] in 10 h, electrolyte: 1 M $LiClO_4$ in PC). b) FTIR spectra recorded at different reduction and oxidation stages during the first cycle. Corresponding c) ^{35}Cl MAS-NMR and d) ^{7}Li MAS-NMR spectra by selecting the OCP point (3.0 V, in blue), at the full reduction (2.0 V, in red) and after a full cycle (3.5 V, in purple).

The ClO_4^- content in the active material was further probed by ^{35}Cl MAS-NMR spectroscopy, which supports the conclusions drawn from the FTIR analysis. Although the signal-to-noise ratio was low, the normalized ^{35}Cl MAS-NMR spectra clearly track the extraction (reduction) and reinsertion (oxidation) of perchlorate anions within the composite (Figure 5c). The spectrum of the pristine electrode (OCP, 3.0 V vs. Li^+/Li) exhibits a single dominant resonance at 998 ppm, attributed to the ClO_4^- anions in the molecular unit. After full reduction at 2.0 V vs. Li^+/Li (i.e., two-electron process), only a minor residual signal at the same chemical shift remains, originating from residual ClO_4^- anions that were not fully extracted, as also observed by FTIR measurements. After full reoxidation at 3.5 V vs. Li^+/Li, the spectrum again displays a resonance at 998 ppm, identical to that of the pristine state. The evolution of the normalized integrated intensity throughout the cycle further supports the good reversibility of perchlorate anion (de)insertion in **(2)**. To monitor the lithium content and to confirm its noninvolvement in the electrochemical process, as shown in Scheme 1, ^7Li MAS-NMR spectroscopy was performed at the same three selected states of charge (Figure 5d). The spectra of the pristine electrode and that obtained after a full electrochemical cycle are very similar, both displaying two broad resonances centered at ≈ −1.4 and −4.4 ppm, respectively. Due to the narrow chemical shift range typically observed for diamagnetic lithium species, precise assignments remain challenging. Nevertheless, these two signals can reasonably be attributed to distinct local lithium environments within the molecular structure. The difference in chemical shift likely reflects slight variations in Li^+ coordination, possibly caused by structural disorder in the molecular packing. The spectrum recorded at 2.0 V vs. Li^+/Li, following the reduction step, still shows two main resonances, now slightly shifted to −1.8 and −3.5 ppm. These small changes are consistent with modest modifications in the local environment of lithium ions due to perchlorate anion extraction, without significant alteration of the carbon-based framework. Comparison of the normalized integrated intensities (with the initial state set to 2 for clarity) reveals no significant change in lithium content throughout the full reduction/oxidation cycle. Indeed, integrated intensities of 2 and 1.9 are measured for spectra recorded at 2.0 V (reduced state) and at 3.5 V (reoxidized state), respectively. In brief, ^7Li MAS-NMR results indicate that Li^+ ions are clearly not involved in the overall electrochemical process.

2.4. Probing the Chemical Conversion of the Neutral [bcbp] (1) into $(Li)_2$[bcbp]$(ClO_4)_2$ Disalt (2) by MAS-NMR

Guided by the MAS-NMR data acquired for **(2)**, we designed an additional experiment to gain deeper insight into the chemical conversion of **(1)** into **(2)**. Ten milligrams of pure compound [bcbp] was placed in contact with the electrolyte using the standard Swagelok cell assembly. After an exposure of 80 h without applying any current, the cell was opened in an argon glovebox, and the recovered powder was rinsed with pure PC and filtered inside the glovebox before being packed into a 2.5 mm outer-diameter MAS-NMR rotor. Both ^{35}Cl MAS and ^7Li NMR spectra were then recorded. A broad signal with a chemical shift close to that of **(2)** was observed (Figure S20, Supporting Information), but the second resonance at −4.4 ppm was not detected. The two resonances in the OCP spectrum (Figure 5d) were assigned to two slightly different Li local environments within the $(Li)_2$[bcbp]$(ClO_4)_2$) framework, most likely arising from molecular stacking in the powder sample. It appears that the limited Li ingress after 80 h of contact resulted in the formation of only one of these environments, highlighting the slow kinetics of the chemical conversion process. On the chlorine side, no signal could be detected probably explained by the lower sensitivity of this nucleus. It is also possible that electrochemical activation is likely required to promote the salt incorporation within the [bcbp] framework.

3. Conclusion

In this study, we synthesized, characterized, and investigated the electrochemical storage properties in Li half-cells of two viologen–carboxylate compounds sharing the same *p*-type redox-active backbone: 1) the double zwitterionic molecule [bcbp] **(1)** and 2) its double zwitterionic $(Li)_2$[bcbp]$(ClO_4)_2$ disalt **(2)**. This work aimed to deepen the understanding of this peculiar class of host materials to promote the development of fully organic anionic batteries. While [bcbp] exhibited initially limited electrochemical activity, it was found to undergo a spontaneous transformation into the electrochemically active disalt **(2)** upon prolonged exposure to the $LiClO_4$-based electrolyte. This time-dependent chemical conversion was confirmed through a combination of electrochemical measurements, FTIR, and EDX analyses. The disalt **(2)** displayed immediately stable and reversible two-step electrochemical behavior characteristic of viologen derivatives with the reversible (de)insertion of perchlorate anions confirmed via ex situ FTIR and $^{35}Cl/^7Li$ MAS-NMR measurements. In addition, we were able to synthesize a radical intermediate **(3)** likely formed during the redox processes and to assess it electrochemically. These results collectively demonstrate that the electrochemical processes occur through perchlorate ion (de) insertion, while the lithium ions remain as spectators of the process, in line with the expected half-reaction mechanism. Overall, our findings highlight the potential of viologen-based double zwitterionic salts as promising *p*-type hosts for anion-driven energy storage systems. The tunability of their redox properties through molecular engineering and ion pairing opens new avenues for the design of next-generation organic electrode materials into the promising domain of anion-rocking-chair batteries.

4. Experimental Section

Synthesis of the Double Zwitterionic 1,1′-Bis(4-Carboxyphenyl)-4,4′-Bipyridinium Hexahydrate Molecule [bcbp] × $6H_2O$ and its Anhydrous Form [bcbp] (1)

The double zwitterionic [bcbp] $6H_2O$ molecule was synthesized by adapting Sui's method[31] to produce a powder of this phase.

Anhydrous $(H)_2[bcbp](Cl)_2$ (200.1 mg, 0.41 mmol, and 1 eq.) was dissolved in 4 mL of ultrapure water in a 25 mL round bottom flask and then heated at 55 °C under stirring for 30 min. A soda solution prepared by dissolving NaOH (34.6 mg, 0.865 mmol, and 2.1 eq.) in 3 mL of ultrapure water was then rapidly added dropwise to the hot $(H)_2[bcbp](Cl)_2$ solution. The resulting homogeneous solution was stirred at 55 °C arbitrary for 18 h. Precipitation occurred after cooling down the solution to room temperature in ambient air. The brown solid was recovered by filtration, washed with ultrapure water, and dried overnight in ambient air; yield 55%.

To prepare the anhydrous [bcbp] phase **(1)**, a typical batch of 100 mg was heated overnight at 150 °C under vacuum in a glass oven (Büchi B-585 Drying), producing a brown powder with the expected mass loss of ≈20% (quant. yield).

Synthesis of the Double Zwitterionic Disalt $(Li)_2[bcbp](ClO_4)_2$ (2)

The double zwitterionic $(Li)_2[bcbp](ClO_4)_2$ disalt was synthesized through acid–base neutralization of $(H)_2[bcbp](ClO_4)_2$, following an adaptation of Walker's protocol.[37] The latter compound was obtained via metathesis of $(H)_2[bcbp](Cl)_2$ (see the Supporting Information). $(H)_2[bcbp](ClO_4)_2$ (150.1 mg, 0.25 mmol, and 1 eq.) was dissolved in 3 mL of MeOH in a 15 mL vial and then maintained at 30 °C under stirring. LiOH $\times H_2O$ (21.1 mg, 0.50 mmol, and 2 eq.) dissolved in 1.9 mL of MeOH was added dropwise to the reaction mixture. After 2 days under stirring, the suspension was centrifuged and the recovered solid was washed with MeOH. The resulting yellow/brown solid was then heated overnight at 170 °C under vacuum in a glass oven (Büchi B-585 Drying), resulting in a color change to green; yield 60%.

Electrochemical Study

Electrochemical measurements were conducted in laboratory two-electrode cells (Swagelok-type cells) following a procedure similar to that previously reported for $(Li)_2[diacetate\text{-}V](ClO_4)_2$.[16] Lithium metal discs were used as negative electrodes, and a single fiberglass separator (Whatman GF/D) soaked with 1 M $LiClO_4$ in PC (≈500 µL) served as the electrolyte unless otherwise specified. Positive electrodes were prepared binder-free in an argon-filled glovebox by manually grinding the active material powders with 33 wt% carbon black (Ketjenblack EC-600JD, AkzoNobel, denoted KB600) using a mortar and pestle. This method provides a simple means to access the essential and intrinsic electrochemical characteristics of the tested active material. The typical composite electrode mass was ≈8 mg. Galvanostatic cycling measurements were conducted with an MPG system (Bio-Logic S.A., Seyssinet-Pariset, France) at 23 °C.

Acknowledgements

A.R. and L.R. contributed equally to this work. This work was realized in the framework of the ANR-DFG project ORGANION (N° ANR-20-CE92-0046-01). It contributes to the research performed at CELEST (Center for Electrochemical Energy Storage Ulm-Karlsruhe) and was funded by the Deutsche Forschungsgemeinschaft (DFG, German Research Foundation) under Project IDs 446026621 (DFG-ANR project ORGANION), 390874152 (POLiS Cluster of Excellence, EXC 2154), 445470598, 445471097, and 445471845. We gratefully acknowledge the support from the CIMEN Electron Microscopy Center in Nantes. Measurements were carried out using the IMN's characterization platform, PLASSMAT, in Nantes, France. Valuable discussions and complementary experimental contributions from Dr. E. Quarez (IMN), A. Florent (IMN) and Dr. B. Collason (LCPBT) are gratefully acknowledged.

Conflict of Interest

The authors declare no conflict of interest.

Data Availability Statement

The data that support the findings of this study are available from the corresponding author upon reasonable request.

Keywords: organic battery · *p*-type organic electrode · viologen · zwitterions

[1] L. Michaelis, E. S. Hill, *J. Gen. Physiol.* **1933**, *16*, 859.
[2] W. Sliwa, B. Bachowska, N. Zelichowicz, *Heterocycles* **1991**, *32*, 2241.
[3] K. Deuchert, S. Hünig, *Angew. Chem., Int. Ed. Engl.* **1978**, *17*, 875.
[4] P. Poizot, J. Gaubicher, S. Renault, L. Dubois, Y. Liang, Y. Yao, *Chem. Rev.* **2020**, *120*, 6490.
[5] C. L. Bird, A. T. Kuhn, *Chem. Soc. Rev.* **1981**, *10*, 49.
[6] J. Ding, C. Zheng, L. Wang, C. Lu, B. Zhang, Y. Chen, M. Li, G. Zhai, X. Zhuang, *J. Mater. Chem. A* **2019**, *7*, 23337.
[7] L. Striepe, T. Baumgartner, *Chem. Eur. J.* **2017**, *23*, 16924.
[8] B. Colasson, T. Devic, J. Gaubicher, C. Martineau-Corcos, P. Poizot, V. Sarou-Kanian, *Chem. Eur. J.* **2021**, *27*, 9589.
[9] R. J. Mortimer, *Annu. Rev. Mater. Res.* **2011**, *41*, 241.
[10] W. Wu, S. Guo, J. Bian, X. He, H. Li, J. Li, *J. Energy Chem.* **2024**, *93*, 453.
[11] M. Kathiresan, B. Ambrose, N. Angulakshmi, D. E. Mathew, D. Sujatha, A. M. Stephan, *J. Mater. Chem. A* **2021**, *9*, 27215.
[12] S. Sen, J. Saraidaridis, S. Y. Kim, G. T. R. Palmore, *ACS Appl. Mater. Interfaces* **2013**, *5*, 7825.
[13] M. Yao, H. Sano, H. Ando, T. Kiyobayashi, *Sci. Rep.* **2015**, *5*, 10962.
[14] K. Hatakeyama-Sato, T. Tezuka, R. Ichinoi, S. Matsumono, K. Sadakuni, K. Oyaizu, *ChemSusChem* **2020**, *13*, 2443.
[15] T. P. Nguyen, A. D. Easley, N. Kang, S. Khan, S.-M. Lim, Y. H. Rezenom, S. Wang, D. K. Tran, J. Fan, R. A. Letteri, X. He, L. Su, C.-H. Yu, J. L. Lutkenhaus, K. L. Wooley, *Nature* **2021**, *593*, 61.
[16] A. Jouhara, E. Quarez, F. Dolhem, M. Armand, N. Dupré, P. Poizot, *Angew. Chem., Int. Ed.* **2019**, *58*, 15680.
[17] V. Cadiou, A. Gaillot, É. Deunf, F. Dolhem, L. Dubois, T. Gutel, P. Poizot, *ChemSusChem* **2020**, *13*, 2345.
[18] M. Bhosale, C. Schmidt, P. Penert, G. Studer, B. Esser, *ChemSusChem* **2024**, *17*, e202301143.
[19] M. Uhl, P. P. Sadeeda, P. A. Schuster, B. W. Schick, S. Muench, A. Farkas, U. S. Schubert, B. Esser, A. J. C. Kuehne, T. Jacob, *ChemSusChem* **2024**, *17*, e202301057.
[20] R. Wessling, H. Koger, F. Otteny, M. Schmidt, A. Semmelmaier, B. Esser, *ACS Appl. Polym. Mater.* **2024**, *6*, 7956.
[21] A. V. Gutov, E. B. Rusanov, A. B. Ryabitskii, I. F. Tsimbal, A. N. Chernega, *Russ. J. Gen. Chem.* **2009**, *79*, 1910.
[22] J.-J. Liu, Y.-F. Guan, M.-J. Lin, C.-C. Huang, W.-X. Dai, *Cryst. Growth Des.* **2015**, *15*, 5040.
[23] M. Leroux, N. Mercier, M. Allain, M.-C. Dul, J. Dittmer, A. H. Kassiba, J.-P. Bellat, G. Weber, I. Bezverkhyy, *Inorg. Chem.* **2016**, *55*, 8587.
[24] M. Leroux, G. Weber, J.-P. Bellat, I. Bezverkhyy, N. Mercier, *Z. Für Anorg. Allg. Chem.* **2016**, *642*, 1439.
[25] Q. Sui, N.-N. Yang, T. Gong, P. Li, Y. Yuan, E.-Q. Gao, L. Wang, *J. Phys. Chem. Lett.* **2017**, *8*, 5450.
[26] R. Rubio-Presa, L. Lubián, M. Borlaf, E. Ventosa, R. Sanz, *ACS Mater. Lett.* **2023**, *5*, 798.
[27] I. S. Chae, M. Koyano, K. Oyaizu, H. Nishide, *J. Mater. Chem. A* **2013**, *1*, 1326.
[28] X. He, L. Chen, T. Baumgartner, *ACS Appl. Mater. Interfaces* **2024**, *16*, 48689.

[29] M. Kato, H. Sano, T. Kiyobayashi, M. Yao, *ChemSusChem* **2020**, *13*, 2379.
[30] O. Toma, M. Leroux, N. Mercier, M. Allain, A. H. Kassiba, S. K. K. Swamy, J. Dittmer, *Eur. J. Inorg. Chem.* **2016**, *2016*, 1036.
[31] Q. Sui, X.-T. Ren, Y.-X. Dai, K. Wang, W.-T. Li, T. Gong, J.-J. Fang, B. Zou, E.-Q. Gao, L. Wang, *Chem. Sci.* **2017**, *8*, 2758.
[32] R. Meziane, J.-P. Bonnet, M. Courty, K. Djellab, M. Armand, *Electrochim. Acta* **2011**, *57*, 14.
[33] R. Bouchet, S. Maria, R. Meziane, A. Aboulaich, L. Lienafa, J.-P. Bonnet, T. N. T. Phan, D. Bertin, D. Gigmes, D. Devaux, R. Denoyel, M. Armand, *Nat. Mater.* **2013**, *12*, 452.
[34] J. Zhu, Z. Zhang, S. Zhao, A. S. Westover, I. Belharouak, P. Cao, *Adv. Energy Mater.* **2021**, *11*, 2003836.
[35] J.-J. Liu, Y.-F. Guan, M.-J. Lin, C.-C. Huang, W.-X. Dai, *Cryst. Growth Des.* **2016**, *16*, 2836.
[36] M. Armand, S. Grugeon, H. Vezin, S. Laruelle, P. Ribière, P. Poizot, J.-M. Tarascon, *Nat. Mater.* **2009**, *8*, 120.
[37] W. Walker, S. Grugeon, H. Vezin, S. Laruelle, M. Armand, F. Wudl, J.-M. Tarascon, *J. Mater. Chem.* **2011**, *21*, 1615.
[38] H. Chen, M. Armand, M. Courty, M. Jiang, C. P. Grey, F. Dolhem, J.-M. Tarascon, P. Poizot, *J. Am. Chem. Soc.* **2009**, *131*, 8984.
[39] L. Bernard, A. Jouhara, E. Quarez, Y. Levieux-Souid, S. L. Caër, P. Tran-Van, S. Renault, P. Poizot, *Inorganics* **2022**, *10*, 62.
[40] A. S. Sajeevan, L. Bernard, P. Tran-Van, D. Brandell, S. Renault, P. Poizot, *ACS Appl. Polym. Mater.* **2024**, *6*, 10102.
[41] J. Peon, X. Tan, J. D. Hoerner, C. Xia, Y. F. Luk, B. Kohler, *J. Phys. Chem. A* **2001**, *105*, 5768.

Manuscript received: June 5, 2025
Revised manuscript received: September 22, 2025
Version of record online: